Supplementary Materials for

Moiré Superlattice Induced Superconductivity in One-unit-cell FeTe

Hailang Qin[1,‡], Xiaobin Chen[2,‡], Bin Guo[1], Tianluo Pan[3], Meng Zhang[1], Bochao Xu[1], Junshu Chen[1], Hongtao He[1], Jiawei Mei[1,3*], Weiqiang Chen[1,4*], Fei Ye[1,3*], Gan Wang[1,4*]

[1]Department of Physics, Southern University of Science and Technology, Shenzhen 518055, China.

[2]School of Science and State Key Laboratory on Tunable Laser Technology and Ministry of Industry and Information Technology Key Lab of Micro-Nano Optoelectronic Information System, Harbin Institute of Technology, Shenzhen 518055, China.

[3]Shenzhen Key Laboratory of Advanced Quantum Functional Materials and Devices, Southern University of Science and Technology，Shenzhen 518055, China.

[4]Guangdong Provincial Key Laboratory of Quantum Science and Engineering, Shenzhen Institute for Quantum Science and Engineering, Southern University of Science and Technology，Shenzhen 518055, China.

[‡]These authors contributed equally to this work: Hailang Qin, Xiaobin Chen.

[*]E-mail: meijw@sustech.edu.cn, chenwq@sustech.edu.cn, yef@sustech.edu.cn, wangg@sustech.edu.cn.

This file includes:

- Experimental and Calculation Details
- **Fig. S1:** The bias dependence of SL.

- **Fig. S2.** Simulated STM images, when the Bi_2Te_3 layer is removed.

- **Fig. S3:** dI/dV spectra on and off the vacancy site.
- **Fig. S4**: STM topographic images of one unit-cell FeTe grown on Bi_2Te_3 thin film under different Te_2/Fe flux ratios.
- **Fig. S5:** The dI/dV mapping showing the effect of sword-shape defect on superconductivity.

1. Experimental and Calculation Details

The substrate is a single crystal 0.7%-wt Nb-doped $SrTiO_3$(001) (STO). The STO substrate was first gradually heated to about 950 ˚C by electron-beam heating and annealed at this temperature for about 30 minutes. The STO substrate was next transferred *in-situ* to an adjacent Createc molecular beam epitaxy (MBE) system for sample growth. The Bi_2Te_3 thin films were first grown by evaporating Bi_2Te_3 compound source with the substrate temperature at about 225 ˚C. The FeTe thin films were then grown by co-evaporation of high purity Fe (99.995%) and Te (99.999%) sources onto the substrate held at around 250 ˚C, unless otherwise specified. For the series of the comparison experiment, three FeTe films was deposited at 250 ˚C with Te_2/Fe flux ratios (by increasing the temperature of Fe source while keeping the temperature of the Te source fixed) of 29, 20, and 11, respectively. The grown samples were then transferred *in-situ* to the SPECS Joule-Thomson (JT) LT-STM system. The base pressure in the MBE chamber and STM chamber was about 3×10^{-10} mbar and 5×10^{-10} mbar, respectively. The STM measurements were performed at 1.1 K (unless

otherwise specified) with etched tungsten tips with the STM bias voltage applied to the sample. The STM tips were sputtered with an Ar^+ ion sputter gun and tested on a reference Au(111) single-crystal. Topographic images were acquired in constant-current mode and dI/dV spectra were measured by using a standard lock-in method with a modulation frequency of 998 Hz and a typical modulation amplitude of 0.1 – 0.5 mV or higher depending voltage range of the spectra. Each spectrum is usually an average of tens of or more spectra acquired at the same location. The STM images were analyzed with WSXM software and there is either no post-processing or only plane and/or flatten operations that are performed for the STM images presented[1]. Brighter in color in an image means higher in value in this study. The thickness of Bi_2Te_3 film used in this study is about 30 nm and the thickness of FeTe is one-unit cell.

Density functional calculations were performed using the projector augmented-wave method [2] as implemented in the Vienna Ab initio Simulation Package (VASP). The General Gradient approximation (GGA) and the Perdew-Burke-Enzerhof-type exchange-correlation functional was adopted [3]. The experimental lattice parameters of $a = b = c = 10.473$ Å and $\alpha = \beta = \gamma = 24.17^{o}$ were adopted for Bi_2Te_3 [4]. The FeTe/Bi_2Te_3 heterostructure was simulated by 3 atomic layers (one-unit-cell) of FeTe placed on top of one quintuple layer (QL) of Bi_2Te_3, where the lower two atomic layers of Bi_2Te_3 were fixed during geometry optimization. The minimal matched lattices of $8 \times 2 \times 1$ FeTe with $7 \times 2 \times 1$ Bi_2Te_3 supercells were employed, where the FeTe monolayer is slightly stretched by 0.4% and compressed by 0.6% along the x and y

directions, respectively. The bicollinear antiferromagnetic state of FeTe is included in the structural optimization. A vacuum layer of about 10 Å was added along the z direction. The Van de Waals interaction was considered by using the optimized exchange Van der Waals functional (optB88-vdW) [5]. The Monkhorst-Pack k mesh sampling was $1 \times 5 \times 1$ (relaxation) and $2 \times 10 \times 1$ (self-consistent run). The energy cutoff was 300 eV and the total energy was deemed converged when the change of energy during the self-consistent run was less than 1×10^{-5} eV. The hybrid structures were optimized until forces acting on the movable atoms were less than 0.01 eV/Å. For the simulation of STM images, the Tersoff-Harman approach was adopted [6].

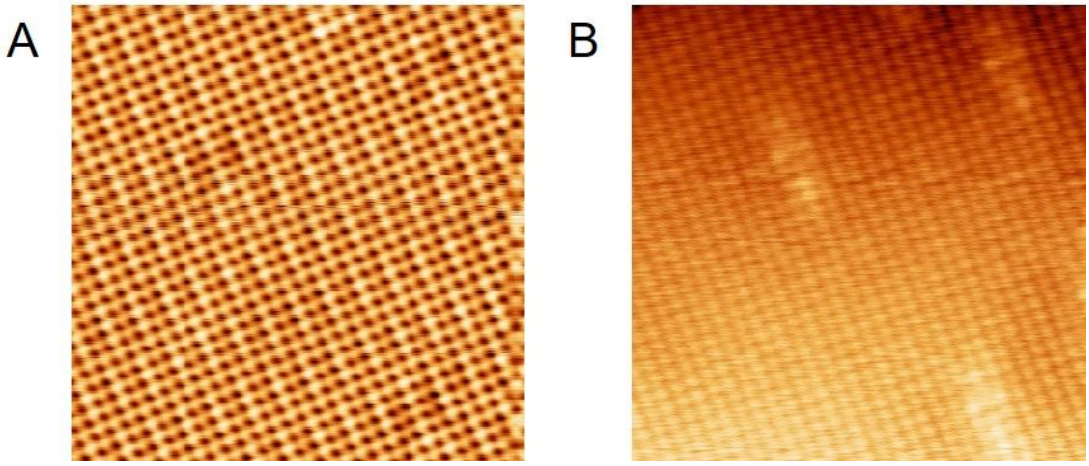

Fig. S1: The bias dependence of SL. (**A**). An STM topographic image at 0.4 V showing a clear SL (size: 10 × 10 nm^2, V_{Bias} = 0.4 V, I_{Tunnel} = 50 pA, color scale: 0.05 nm) (**B**). The STM topographic image of the same area as that in (A) at a different bias (size: 10 × 10 nm^2, V_{Bias} = 5 mV, I_{Tunnel} = 50 pA, color scale: 0.2 nm), in which the SL is not clear.

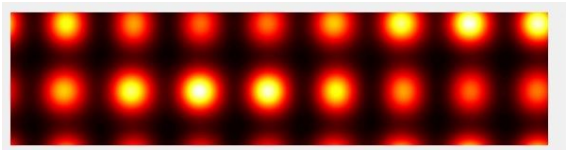

Fig. S2. Simulated STM images, when the Bi_2Te_3 layer is removed. Simulated STM images at 0.1 V, when the Bi_2Te_3 layer is removed, keeping the FeTe the same structure as that after structural relaxation.

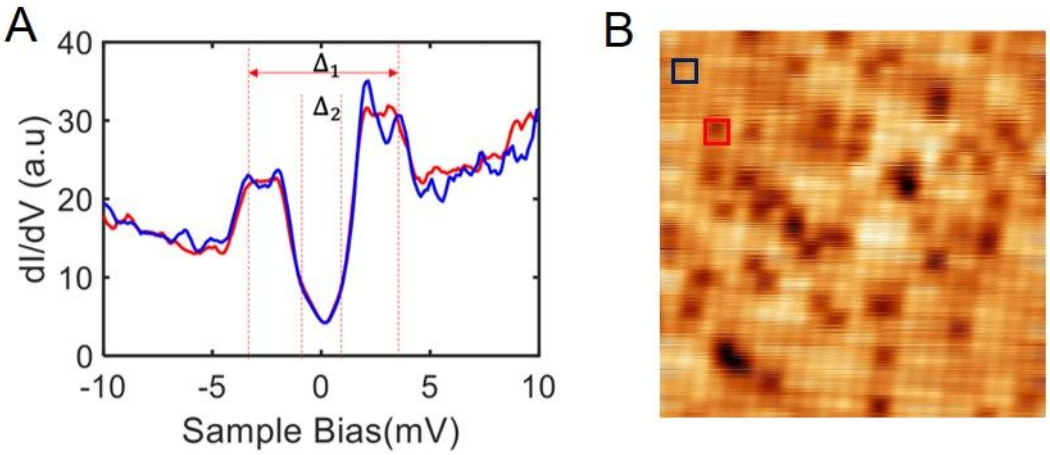

Fig. S3: dI/dV spectra on and off the vacancy site. (A) dI/dV spectra obtained on (the red spectrum) and off (the blue spectrum) a vacancy site with two superconducting gaps nearly identical to each other. (**B**) a vacancy rich region for obtaining the superconducting spectra shown in (a) with red and blue squares indicating the spectra sites (size: 8 × 8 nm^2, setpoint: V_{Bias} = – 10 mV, I_{Tunnel} = 1 nA, color scale: 0.06 nm).

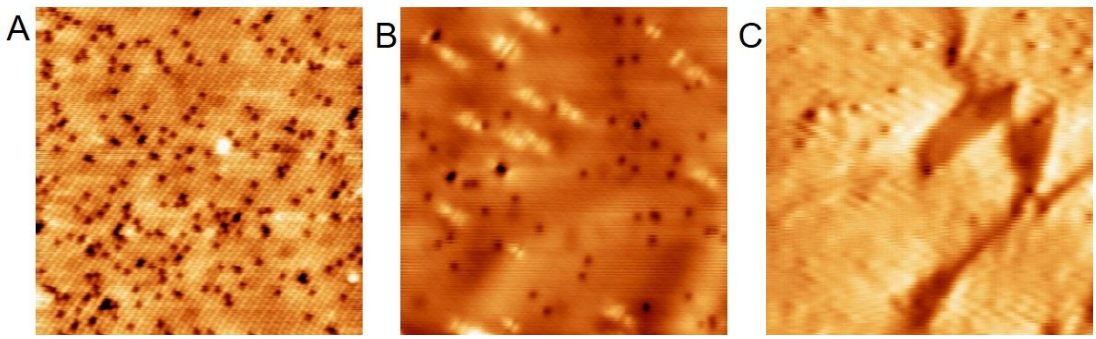

Fig. S4: STM topographic images of one unit-cell FeTe grown on Bi_2Te_3 thin film under different Te_2/Fe flux ratios. (**A**). Flux ratio of about 35 (Fe: 1270 ˚C, Te: 350 ˚C, size: 20 × 20 nm^2, setpoint: V_{Bias} = – 20 mV, I_{Tunnel} = 200 pA, color scale: 0.10 nm, image acquired at 77 K). (**B**). Flux ratio of about 23 (Fe: 1300 ˚C, Te: 350 ˚C, size: 20 × 20 nm^2, setpoint: V_{Bias} = – 20 mV, I_{Tunnel} = 900 pA, color scale: 0.06 nm, image acquired at 4.5 K). (**C**). Flux ratio of about 11 (Fe: 1350 ˚C, Te: 350 ˚C, size: 20 × 20 nm^2, setpoint: V_{Bias} = – 20 mV, I_{Tunnel} = 3 nA, color scale: 0.15 nm, image acquired at 4.5 K).

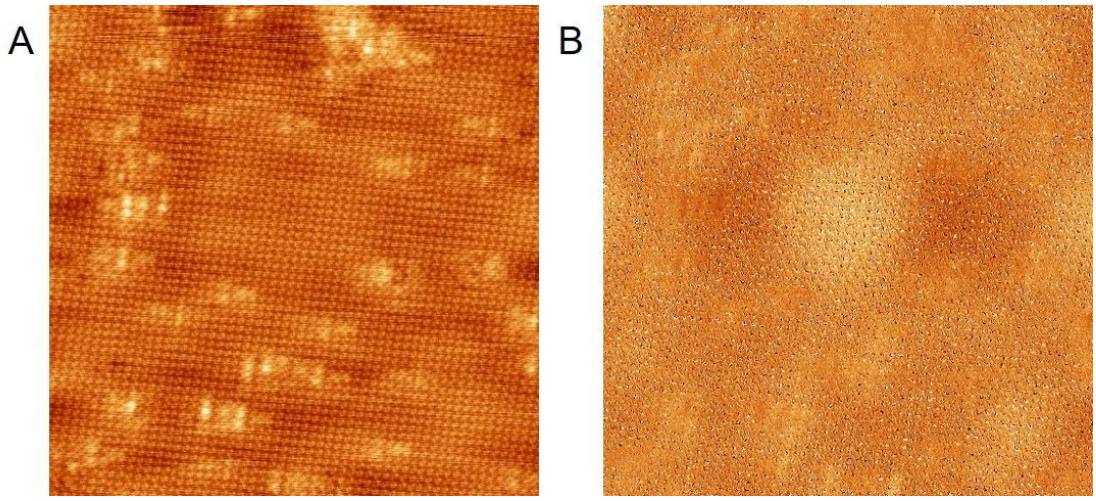

Fig. S5: The dI/dV mapping showing the effect of sword-shape defects on superconductivity. (**A**) An STM topographic image with a substantial number of sword-shape defects (size: 20 × 20 nm^2, V_{Bias} = 3.1 mV, I_{Tunnel} = 50 pA, color scale: 0.1 nm). Note that the defects' shapes are not as clear as those in the main manuscript mainly because the tip was not at its optimal condition and the scanning was especially slow in order to obtain a nice dI/dV image. (**B**) Corresponding dI/dV map (size: 20 × 20 nm^2, V_{Bias} = 3.1 mV, I_{Tunnel} = 50 pA) of (A).

References

1 I. Horcas, R. Fernández, J. M. Gómez-Rodríguez, J. Colchero, J. Gómez-Herrero and A. M. Baro. WSXM: A software for scanning probe microscopy and a tool for nanotechnology. *Rev. Sci. Instrum.* **78**, 013705, (2007).

2 P. E. Blöchl. Projector augmented-wave method. *Phys. Rev. B* **50**, 17953-17979 (1994).

3 J. P. Perdew, K. Burke and M. Ernzerhof. Generalized Gradient Approximation Made Simple. *Phys. Rev. Lett.* **77**, 3865-3868 (1996).

4 R. W. G. Wyckoff. *Crystal Structures*. Vol. 2 (J. Wiley and Sons, 1964).

5 M. Dion, H. Rydberg, E. Schröder, D. C. Langreth and B. I. Lundqvist. Van der Waals Density Functional for General Geometries. *Phys. Rev. Lett.* **92**, 246401, (2004).

6 J. Tersoff and D. Hamann. Theory and application for the scanning tunneling microscope. *Phys. Rev. Lett.* **50**, 1998 (1983).